EVS25
Shenzhen, China, Nov 5-9, 2010

The Electrochemical Behavior of $LiFePO_4$/C Cathode Materials Doped with Antimony

George Ting-Kuo Fey[1*], Po-Yu Peng[1], Kai-Pin Huang[1], Yi-Chuan Lin[1], Yung-Da Cho[1], Hsien-Ming Kao[2]

[1]*Department of Chemical and Materials Engineering, National Central University, Chung-Li, Taiwan 32054, R.O.C*

[2]*Department of Chemistry, National Central University, Chung-Li, Taiwan 32054, R.O.C*

**gfey@cc.ncu.edu.tw*

Abstract

$LiFePO_4$ is considered as a practical cathode material because of low raw materials' cost, excellent thermal safety, environmental friendliness, and long operational life, despite obstacles such as low tap density, low electric conductivity and slow lithium-ion diffusion. To overcome these problems, we used an antimony-ion doping method to synthesize $LiFePO_4$/C with sebacic acid as a carbon source by a high-temperature solid-state reaction method. The effects of antimony concentration, sebacic acid content, calcination temperature, and calcination time on cell performance were investigated. After Sb^{3+} doping, $LiFePO_4$ was converted to a p-type semiconductor and demonstrated greater electric conductivity of about 10^{-3} S cm^{-1}. The 1.0 mol.% Sb-doped $LiFePO_4$/C synthesized with 36 wt.% sebacic acid delivered an initial discharge capacity of 154 mAh g^{-1} at a 0.2 C-rate between 4.0-2.8 V. The doped cathode materials were further characterized by X-ray diffractometer (XRD), scanning electron microscope (SEM), and high-resolution transmission electron microscope (TEM) techniques for structural analysis and confirmation.

Keywords: *$LiFePO_4$, antimony doping, sebacic acid, high-temperature solid-state method, Li-ion batteries*

1 Introduction

In recent years, lithium-ion batteries have attracted significant interest in the energy storage of 3C applications, because of their high energy density, absence of memory effect, and long shelf life. The commercial cathode material of lithium-ion batteries, $LiCoO_2$, provides high potentials (above 4 V vs. Li/Li^+) and good reversible capacities over 150 mAh g^{-1} in practical uses. However, safer, lower-cost and higher-power cathode materials are required for many applications such as EVs and HEVs. [1]

Olivine $LiFePO_4$, which was first developed by Goodenough and his co-workers in 1997 [2], has been demonstrated as one of the most promising cathode materials due to its environmental friendliness, high theoretical capacity (170 mAh g^{-1}) [3-5], high charge/discharge potential (3.4 V

versus Li^+/Li) [6,7], long cycle life [8-10], good thermal stability [11], low raw materials' cost [12-15], and high energy density [6,16].

It is known that $Li_{1-x}FePO_4$ compositions are composed of $LiFePO_4$ and $FePO_4$ phases, both of which seem to be insulating as a result of the single iron valency of Fe^{2+} and Fe^{3+}, respectively[2,17]. Due to the intrinsic poor electronic conductivity ($10^{-10} \sim 10^{-9}$ S cm^{-1}) [18] and low Li^+ diffusion coefficient (1.8×10^{-14} S cm^{-1}) [19] of pristine $LiFePO_4$, it is difficult to reach its full theoretical capacity at useful rates. To overcome these problems, many research groups have used various methods, such as surface carbon coating [20-22], cation doping [23-25], and particle-size optimizing [26-28].

In 2002, Chung [23] converted $LiFePO_4$ to a p-type semiconductor to increase its electrical conductivity enormously by doping $LiFePO_4$ with supervalent cations. Since then, various metal doping sources of $LiFePO_4$ have been widely studied, such as Co [29,30], Cr [31,32], Mg [33,34], Al [35,36], Mn [37, 38], Mo [39], Zn [40], Nb [23] ,Ti [23] and Zr [23]. However, there are no reports on the electrochemical properties of antimony-doped $LiFePO_4$.

In this work, we have prepared $LiFe_{1-x}Sb_xPO_4/C$ (x=0.008, 0.010, 0.012, 0.014) composites by using a simple high-temperature solid-state method in the presence of sebacic acid as a carbon source. The electrochemical behavior of the Sb-doped $LiFePO_4/C$ composites was investigated.

2 Experimental

2.1 The in-house synthesis of $LiFe_{1-x}Sb_xPO_4$

The $LiFe_{1-x}Sb_xPO_4$ powders were prepared using lithium carbonate (Merck, 99%), iron(II) oxalate dehydrate (Showa, 98%), antimony oxide (Sigma, 99%), and ammonium dihydrogen phosphate(Sigma, 99%) in a stoichiometric molar ratio (1.03 : 1-x : x : 1). The starting materials were mixed and ground in a planetary ball-mill with a rotation speed of 250 rpm for 3 h in acetone under an argon atmosphere. Then, the mixture was preheated at 593K at a 5 K min^{-1} heating rate and held at 593 K for 10 h under an Ar/H_2 (v/v 95:5) atmosphere, in order to obtain gray $LiFe_{1-x}Sb_xPO_4$ precursor powders. Before final sintering, we mixed the precursor of $LiFe_{1-x}Sb_xPO_4$ with a proper quantity of sebacic acid (Acros, 98%), and then the mixture was heated in a quartz-tube furnace at 873 K under a flowing Ar/H_2 (v/v 95:5) atmosphere for 12 h.

2.2 Characterization

We used a powder X-ray diffractometer (XRD), Siemens D-5000, Mac Science MXP18, equipped with a nickel-filtered Cu K radiation source (λ= 1.5405 Å), to analyze the structure of materials. The diffraction patterns were recorded between scattering angles of 15° and 80° in steps of 0.05°. The morphology of the $LiFe_{1-x}Sb_xPO_4/C$ composite was observed with a scanning electron microscope (SEM; Hitachi S-3500V) and high-resolution transmission electron microscope (HR-TEM; Jeol TEM-2000FXII). Electron diffraction patterns were obtained through selected area electron diffraction (SAED). The chemical composition of the separated phases was determined by nano beam energy dispersive spectroscopy (EDS). For these experiments, samples were previously dispersed in acetone and deposited on a holey silicon grid. Carbon content analysis of the products was investigated on a OIA Model Solids module as the total organic carbon (TOC) analyzer. Conductivity was measured by four-point conductivity measurements with a Keithley Model 2400S source meter.

2.3 Electrochemical characterization

The cathode was prepared by mixing 85 wt.% carbon-coated $LiFe_{1-x}Sb_xPO_4$ powder with 10 wt.% conductive carbon black and 5 wt.% polyvinylidene fluoride (PVDF) in n-methyl-2-pyrrolidone (NMP) solution. The as-prepared slurry was applied to cover an etched aluminum foil current collector and dried at 393 K for 12 h in an oven. Lithium metal (Foote Mineral) was used as the anode and a 1 M solution of $LiPF_6$ in EC:DEC(1:1 v/v) (Tomiyama Chemicals) was used as the electrolyte with a Celgard membrane as the separator. The cells were assembled in an argon-filled (VAC MO40-1 glove box). The cells were galvanostatically charged and discharged between 2.8 and 4.0 V at a 0.2 C-rate or 2.0 and 4.6 V at different current densities on the electrochemical instrument (Maccor 4000).

3 Results and discussion

3.1 XRD analysis

The XRD patterns of $LiFe_{1-x}Sb_xPO_4/C$ composites (x= 0, 0.008, 0.010, 0.012, 0.014) are shown in Fig.1. The Sb-doped samples are consistent with the standard JCPDS pattern of $LiFePO_4$ (JCPDS (40-1499) $LiFePO_4$), and there was no impurity peaks such as Fe_2O_3 or Fe_2P detected on the $LiFe_{1-}$

$_xSb_xPO_4$/C samples, which reveals that the original olivine structure remained crystalline and intact during the doping process [41]. By using the Scherrer's formula:

$$\beta\cos(\theta)=k\lambda/D \quad (1)$$

We can calculate the grain size (D), where β is the full-width-at-half-maximum length of the (0 2 0) reflection [42] and k is a constant here close to unity. The mean values (D) of $LiFePO_4$/C and $LiFe_{0.99}Sb_{0.01}PO_4$ are 29.3 and 23.6 nm, respectively, which shows that the particle size of the doped composite powder was restrained in our doping process.

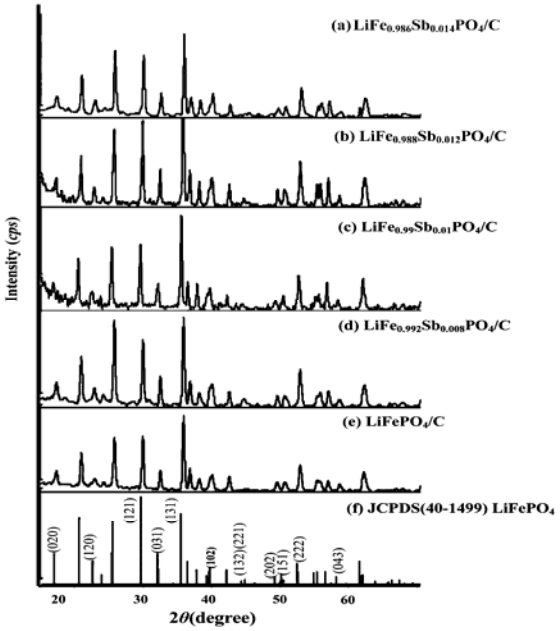

Figure 1: XRD patterns of 36 wt.% sebacic acid–coated $LiFe_{1-x}Sb_xPO_4$. (a) x=0.014, (b) 0.012, (c) 0.010, (d) 0.008, (e) 0.000 , (f) JCPDS pattern (40-1499) of $LiFePO_4$

X-ray diffraction patterns of $LiFe_{0.99}Sb_{0.01}PO_4$/C powders sintered for 12 h at different temperatures from 823 K to 973 K are shown in Fig. 2. It is obvious that the peaks become sharper when temperature increases due to the highly crystalline structure. From Scherrer's formula, the grain sizes of the $LiFe_{0.99}Sb_{0.01}PO_4$/C samples with different sintering temperatures (T= 823, 873, 923, 973 K) were 17.0, 23.6, 24.6, and 26.5 nm, respectively. The grain sizes show that higher temperatures result in larger grain size. However, the impurity phase Fe_2P around 2θ =45◦ and 50◦ was detected in the sample prepared above 923 K (see Fig. 2 (c) and (d)). Ojczyk et al.[43] have reported that Fe_2P can enhance the electronic conductivity and rate performance of $LiFePO_4$/C.

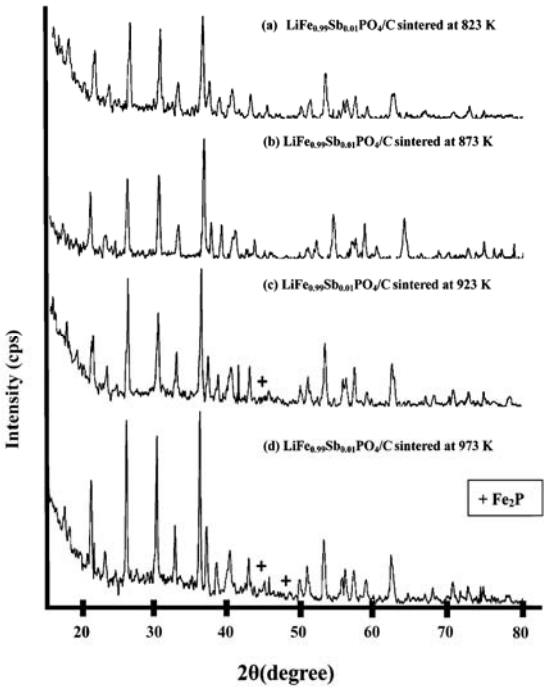

Figure 2: XRD patterns of 36 wt.% sebacic acid–coated $LiFe_{0.99}Sb_{0.01}PO_4$ at different sintering temperatures.

3.2 Carbon content analysis

The real carbon content in the $LiFe_{0.99}Sb_{0.01}PO_4$/C composite was analyzed by total organic carbon (TOC) determination. Samples were pressed into disk-shaped pellets and their electronic conductivity was measured by the four-point dc method. Table 1 shows the comparison of TOC, initial discharge capacity, and conductivity of the $LiFe_{0.99}Sb_{0.01}PO_4$/C composites when different quantities of sebacic acid were used. We can see that when more sebacic acid used, more real carbon content was obtained. In addition, the conductivity of the sample had an increasing trend with higher carbon content. However, the initial discharge capacity didn't follow this trend.

Table 1: A comparison of total carbon content, initial discharge capacity, and electronic conductivity of $LiFe_{0.99}Sb_{0.01}PO_4$/C composites treated with different quantities of sebacic acid.

Sebacic Acid Concentration	TOC	Initial Discharge Capacity	Electronic Conductivity	Preparation Condition
	[wt.%]	[mAh g^{-1}]	[S cm^{-1}]	
34 wt.% Sebacic Acid	2.13	146	4.84×10^{-4}	1.0 mole% Sb 873 K 12 h
36 wt.% Sebacic Acid	2.73	154	9.81×10^{-4}	
38 wt.% Sebacic Acid	3.32	146	1.25×10^{-3}	
40 wt.% Sebacic Acid	3.94	143	2.33×10^{-3}	

3.3 Morphology

The size distribution and morphology of the $LiFe_{0.99}Sb_{0.01}PO_4/C$ particles were studied by a scanning electron microscope (SEM) on a Hitachi model: S-3500N equipped with an energy dispersive spectrometer, which was used to determine the elemental distribution. Fig. 3 (a) and (b) show SEM images of the $LiFe_{0.99}Sb_{0.01}PO_4/C$ composite sintered at 873 K for 12 hours. The samples were mainly fine particles between 150 and 200 nm in size, and we can find some agglomerations of the sample due to the formation of secondary particles.

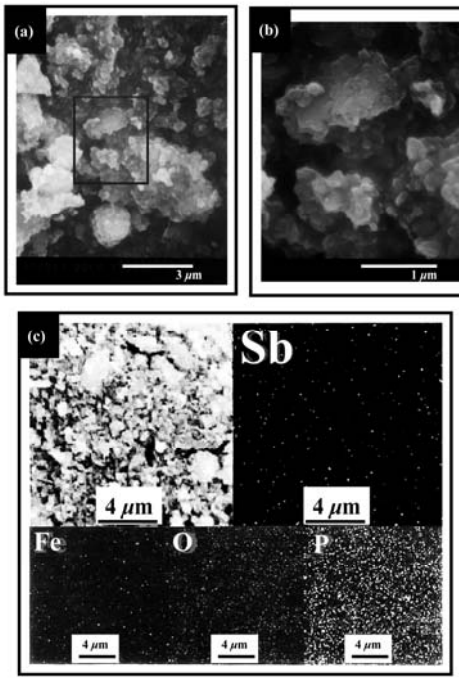

Figure 3: (a)-(b) SEM micrographs of $LiFe_{0.99}Sb_{0.01}PO_4/C$ powders ; (c) elemental mapping of $LiFe_{0.99}Sb_{0.01}PO_4/C$ powders

The SEM and EDS mapping images (Sb, Fe, P, and O) of $LiFe_{0.99}Sb_{0.01}PO_4/C$ are shown in Fig. 3 (c). The distribution areas for elements (Sb, Fe, P and O) are homogeneous. There is also a uniform distribution of the Sb-dopant element on the surface of $LiFe_{0.99}Sb_{0.01}PO_4/C$. Fig. 4 shows the SEM analysis of $LiFe_{0.99}Sb_{0.01}PO_4/C$ at various sintering temperatures. The particle sizes of $LiFe_{0.99}Sb_{0.01}PO_4/C$ treated at 823, 873, 923, and 973 K were 100-150, 150-200, 250-400, and 300-500 nm, respectively. It is clear that higher sintering temperature leads to larger average particle sizes, which is consistent with XRD analysis. However, these values are quite different from those calculated by Scherrer's formula, indicating the primary particles agglomerate to secondary particles. The same result was also reported by Kwon et al. [44]. Larger grain size should lead to greater polarization and lower the capacity of $LiFePO_4/C$.

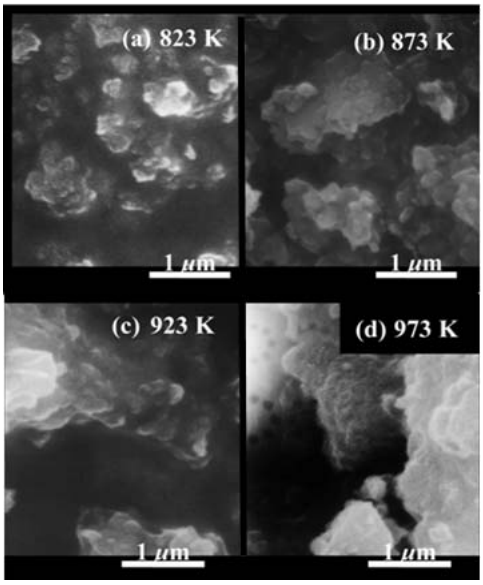

Figure 4: SEM micrographs of $LiFe_{0.99}Sb_{0.01}PO_4/C$ at different sintering temperatures.

3.4 TEM/SAED/EDS analysis

To analyze the morphology of $LiFe_{0.99}Sb_{0.01}PO_4/C$ particles and the carbon coating layer on the particle surface in detail, we used TEM in combination with SAED and EDS. Fig.5 (a) and (b) display the TEM images of the $LiFe_{0.99}Sb_{0.01}PO_4/C$ samples. In the micrographs, we can see that independent particles are packed closely, and all of the samples are well-covered with a carbon layer. The average particle sizes of $LiFe_{0.99}Sb_{0.01}PO_4/C$ composites are around 100~ 150 nm with a carbon layer about 10~ 20 nm thick on the surface.
Fig. 5 (c) and (d) are the SAED analysis images of regions I and II in Fig. 5(b), respectively. Likewise, Fig. 5 (e) and (f) are the EDS analysis images of regions I and II in Fig. 5 (b), respectively.
The SAED analysis images show a bright spot on the outer carbon layer (region I) of $LiFe_{0.99}Sb_{0.01}PO_4/C$ in Fig. 5 (c), which indicates that the carbon layer had a disordered carbon structure. The dark region (region II) shows a bright spot pattern in Fig. 5 (d), which is typical for crystalline $LiFePO_4$. From these results, we conclude that the outer layer (region I) is amorphous carbon, and the inner particle (region II) is crystalline $LiFePO_4$, both of which are consistent with our previous findings [45].

To prove antimony doping in the $LiFePO_4$ particles, EDS analysis was used. The EDS images, Fig. 5 (e) and (f), confirmed that the transparent layer (region I) was mainly carbon (Fig. 5 (e)) and the dark area (region II) included the main elements such as Fe, P, O and Sb elements (Fig. 5 (f)).

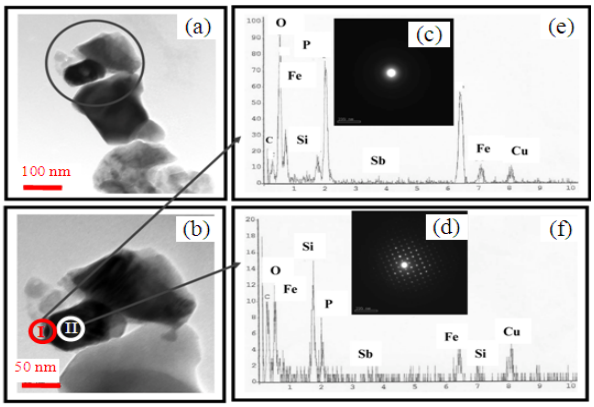

Figure 5: (a)–(b) TEM micrographs of $LiFe_{0.99}Sb_{0.01}PO_4/C$ powders; (c)–(d) SAED for the $LiFe_{0.99}Sb_{0.01}PO_4/C$ particles; (e)–(f) EDS analysis for the $LiFe_{0.99}Sb_{0.01}PO_4/C$ particles

3.5 Electrochemical properties

Table 2 shows a comparison of electronic conductivity and initial discharge capacity of $LiFe_{1-x}Sb_xPO_4$/Ccomposites treated with 36 wt.% sebacic acid at various Sb-doping concentrations (x=0, 0.008, 0.010, 0.012, 0.014). Conductivity increased with increasing antimony doping concentrations, which implies that antimony doping could improve the conductivity of the $LiFePO_4$ cathode material. However, the higher Sb-doping concentration did not result in higher initial discharge capacity. Therefore, an appropriate doping level is a very important consideration. According to Xie and Zhou [46], the multivalent metal ion locating in lithium sites improves electronic conductivity of the material, but lithium ion diffusion may be hindered if too many lithium sites are occupied with multivalent metal ion, so excess antimony doping would disturb the tunnels of lithium ions and impede Li^+ diffusion of $LiFePO_4$.

The capacity and cyclability of $LiFe_{1-x}Sb_xPO_4/C$ samples (x=0, 0.008, 0.010, 0.012, 0.014) were determined between 4.0 and 2.8 V by galvanostatic charge/discharge tests at a 0.2 *C*-rate. Fig. 6 demonstrates the effect of antimony concentration on discharge capacity, while Fig. 7 shows the charge/discharge voltage profiles at the first cycle. At the optimum Sb-doping concentration (x=0.01) in Fig. 6, the $LiFe_{0.99}Sb_{0.01}PO_4/C$ sample shows the highest initial discharge capacity of 155 mAh g^{-1} due to the appropriate antimony content that increased electronic conductivity (see Table.1, 8.76×10^{-4} S cm^{-1}) and minimized the polarization between lithium extraction and insertion. In this case, the $LiFe_{0.99}Sb_{0.01}PO_4/C$ composite delivered a high capacity because its conductivity was improved by a conversion to p-type semi-conductivity via a dopant effect [23].

Table 2: A comparison of initial discharge capacity and electronic conductivity of $LiFe_{1-x}Sb_xPO_4/C$ (x=0, 0.008, 0.010, 0.012, 0.014) composites treated with 36 wt.% sebacic acid.

Sb-doping Concentration	Electronic Conductivity [S cm^{-1}]	Initial Discharge Capacity [mAh g^{-1}]	Preparation Condition
0 mole% Sb-doped	5.87×10^{-5}	126	
0.8 mole% Sb-doped	1.84×10^{-4}	140	36 wt.% Sebacic Acid
1.0 mole% Sb-doped	8.76×10^{-4}	154	873 K
1.2 mole% Sb-doped	9.81×10^{-4}	142	12 h
1.4 mole% Sb-doped	2.33×10^{-3}	141	

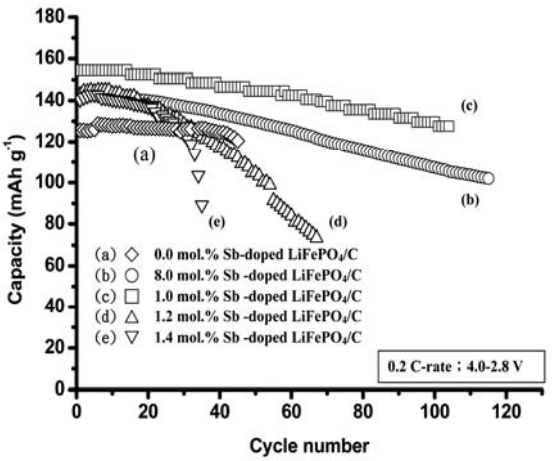

Figure 6: Galvanostatic cycling performance of $LiFe_{1-x}Sb_xPO_4/C$ (x=0, 0.008, 0.010, 0.012, 0.014) composites treated with 36 wt.% sebacic acid and doped with different Sb concentrations.

In Fig.7, all the samples displayed flat charge and discharge voltage plateaus around 3.5 and 3.4 V, respectively. The voltage difference between charge and discharge plateaus (ΔV) is related to the polarization of the cell system. The lower polarization comes with the smaller ΔV. As shown in Fig. 7, an undoped sample exhibits the largest ΔV of 0.154 V compared to that of 0.097 V for $LiFe_{0.99}Sb_{0.01}PO_4/C$. The good cycling performance of the doped composite was partly attributed to its low polarization.

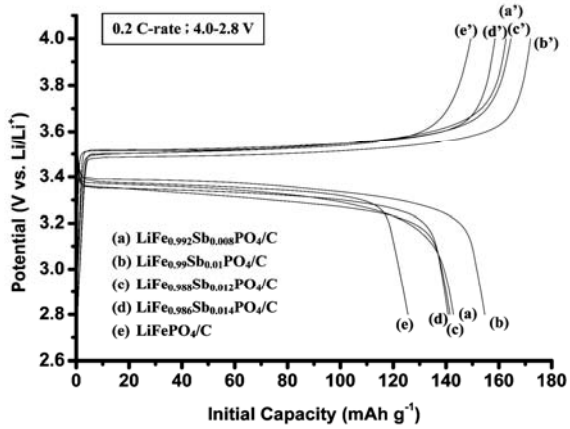

Figure 7: Initial charge and discharge curves for bare $LiFePO_4$ and $LiFe_{1-x}Sb_xPO_4/C$ materials treated with 36 wt.% sebacic acid. (a)–(e): discharge; (a')–(e'): charge

Sebacic acid was used as the carbon source for the preparation of composite cathode material and a proper quantity was critical to the electrode performance. Fig. 8 displays the effects of sebacic acid concentrations on the discharge capacities, while Fig. 9 shows the concentration effects on charge/discharge voltage profiles at the first cycle.

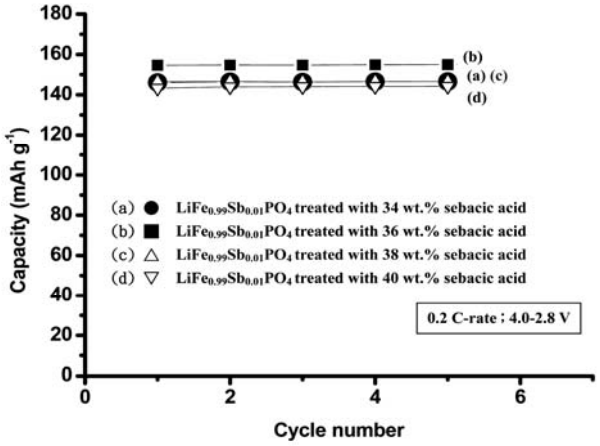

Figure 8: Discharge capacity vs. cycle number for $LiFe_{0.99}Sb_{0.01}PO_4/C$ treated with various wt.% of sebacic acid.

The $LiFe_{0.99}Sb_{0.01}PO_4/C$ samples were individually treated with 34, 36, 38, and 40 wt.% sebacic acid. It is clear from these figures that $LiFe_{0.99}Sb_{0.01}PO_4/C$ treated with 36 wt.% sebacic acid exhibited the best discharge performance and the smallest ΔV between charge and discharge plateaus. However, the best discharge capacity did not come with the highest electronic conductivity, as shown in Table 1, probably due to the large amount of electro-inactive material.

The influence of sintering temperature and duration on $LiFe_{0.99}Sb_{0.01}PO_4$ with 36 wt.% sebacic acid is shown in Fig. 10 and Fig. 11. $LiFe_{0.99}Sb_{0.01}PO_4$ sintered at 873 K had the highest capacity of 154 mAh g^{-1} during the first five cycles. Based on the work of Yamada et al. [26] and Kwon et al. [44], the $LiFePO_4$ particles would agglomerate under a high temperature environment and particle growth led to a smaller surface area on $LiFe_{0.99}Sb_{0.01}PO_4/C$ and an increase in polarization due to the diminishing $LiFePO_4/FePO_4$ interface. On the other hand, lower temperatures resulted in finer particles, but influenced the crystallinity of $LiFe_{0.99}Sb_{0.01}PO_4/C$.

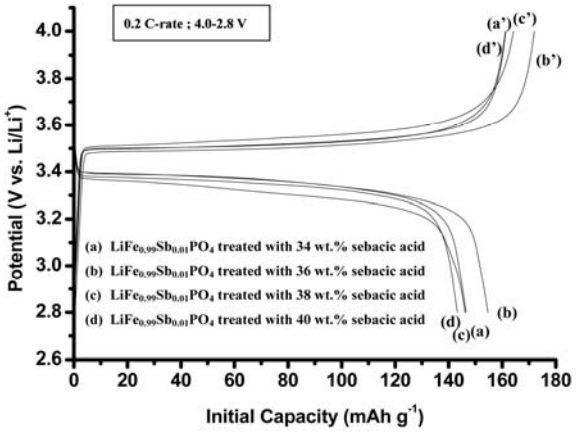

Figure 9: Initial charge and discharge curves for $LiFe_{0.99}Sb_{0.01}PO_4/C$ composites treated with various wt.% of sebacic acid.(a)–(d): discharge; (a')–(d'): charge

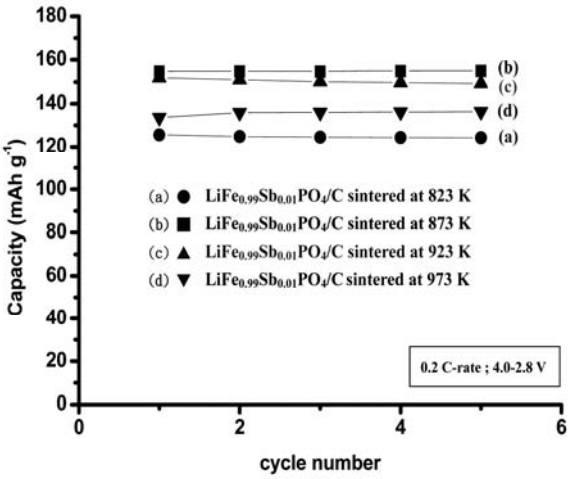

Figure 10: Discharge capacity vs. cycle number for $LiFe_{0.99}Sb_{0.01}PO_4$ at different sintering temperatures.

In addition, sintering time also plays an important part on particle size and crystallinity. Fig. 11 exhibits a comparison of the $LiFe_{0.99}Sb_{0.01}PO_4/C$ composites treated with various sintering durations (4, 8, 12, 16, 20 h). Longer sintering time led to larger particle size and better crystallinity. However, this does not mean that long sintering time produces a better cathode material, because large particles cause a reduction in surface area and a diffusion limit of lithium ions. Based on the data from Fig.11, a suitable sintering time might be 8 h for synthesizing $LiFe_{0.99}Sb_{0.01}PO_4/C$.

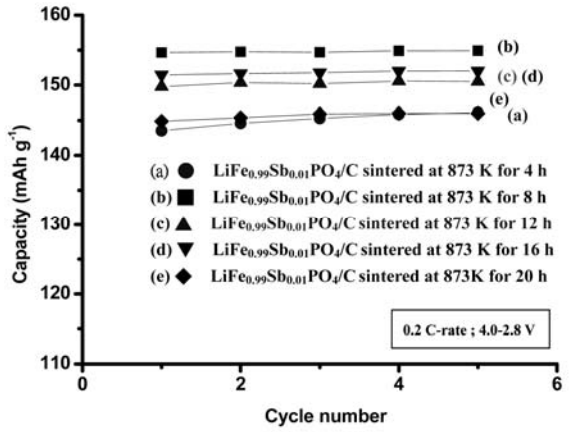

Figure 11: Discharge capacity vs. cycle number for $LiFe_{0.99}Sb_{0.01}PO_4$ at different sintering duration conditions

Fig. 12 represents the rate capability of $LiFePO_4/C$ and $LiFe_{0.99}Sb_{0.01}PO_4/C$ samples between 4.0-2.8 V. The discharge capacities of $LiFePO_4/C$ and $LiFe_{0.99}Sb_{0.01}PO_4/C$ are 30 and 5 mAh g^{-1} at 4 C, respectively. We found that Sb-doping did improve the rate capability due to the enhanced electronic conductivity.

In Fig.13, the discharge capacities of $LiFe_{0.99}Sb_{0.01}PO_4/C$ sintered at 823 K, 873 K, 923 K, and 973 K are 125, 154, 151 and 143 mAh g^{-1} at 0.2 C-rate, respectively, and 0, 0, 2, and 26 mAh g^{-1} at 8 C-rate, respectively. It was impressive that higher rate capability accompanied the higher sintering temperature between 823 K and 973 K. The $LiFe_{0.99}Sb_{0.01}PO_4/C$ treated at 973 K has the best rate capability, since the formation of Fe_2P improved the electronic conductivity of $LiFe_{0.99}Sb_{0.01}PO_4/C$. Even though the higher sintering temperature of $LiFePO_4/C$ leads to larger particle size and loss of capacity as reported by our previous report [47], electronic conductivity is the main factor determining rate capability of $LiFe_{0.99}Sb_{0.01}PO_4/C$. Kang [48] also reported that the best sintering temperature of $LiFePO_4/C$ was 973 K due to the formation of Fe_2P.

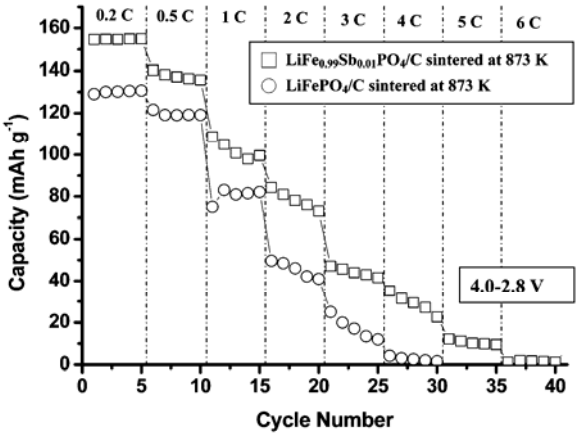

Figure 12: A comparison of the rate performance between Sb-doped and Sb-undoped $LiFePO_4/C$ composites treated at 873K. (Charge/discharge: 4.0/2.8 V)

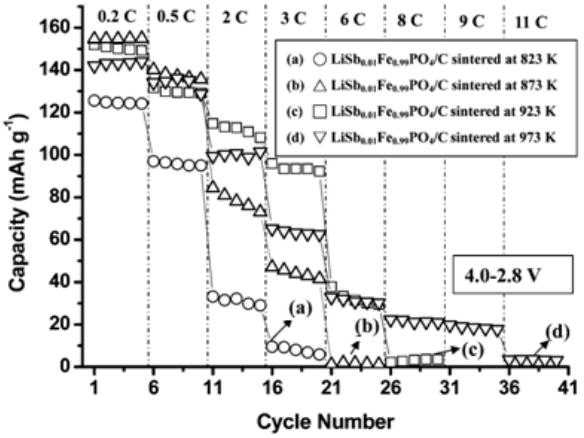

Figure 13: The rate performance of $LiFe_{0.99}Sb_{0.01}PO_4/C$ composites sintered at different temperatures. (Charge/discharge: 4.0/2.8 V)

Because high current density would increase the charge/discharge polarization voltage which could mask the true rate capability of the material, we changed the charge/discharge cut-off voltage range from 4.0-2.8 V to 4.6-2.0 V, as shown in Fig. 14. Again, this figure clearly demonstrates that Sb-doping can significantly improve the high rate performance of the material due to enhanced electronic conductivity.

Fig. 15 displays the discharge behavior of $LiFe_{0.99}Sb_{0.01}PO_4/C$ sintered at 973 K in the cut-off potential range of 4.6-2.0 V. After the first series of c-rate tests from 0.2 C to 28 C in Fig. 15, we continued the second series and found that the discharge capacity at a 0.2 C-rate was 150 mAh g^{-1},

which was almost the same as the first series. This means that the $LiFe_{0.99}Sb_{0.01}PO_4/C$ structure remained stable after high rate tests.

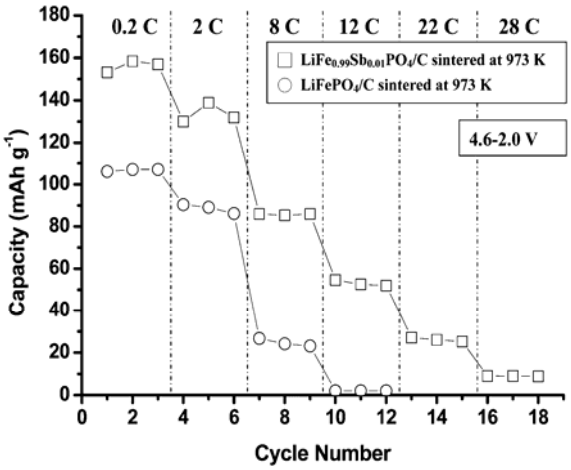

Figure 14: A comparison of the rate performance between Sb-doped and Sb-undoped $LiFePO_4/C$ composites treated at 973K. (Charge/discharge: 4.6/2.0 V)

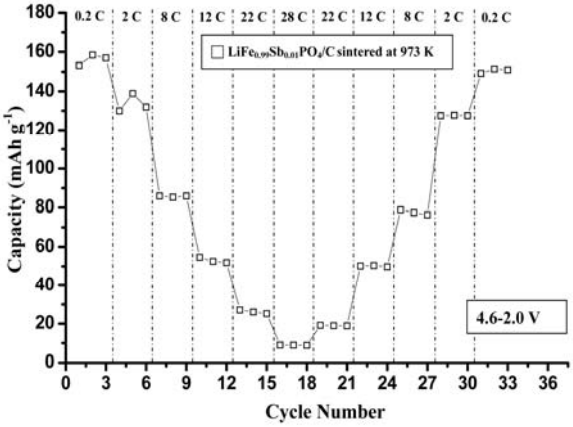

Figure 15: The rate performance of $LiFe_{0.99}Sb_{0.01}PO_4/C$ at 973 K in the range of cut-off voltages: 4.6/2.0 V.

In Fig. 16, the charge/discharge voltage profile exhibits that the charge/discharge voltage plateaus for 0.2 C and 12 C are around 3.5/3.4 V and 4.0/3.0 V, respectively, which proves that the high charge voltage plateau can restrict the charge/discharge test, and this cut-off voltage range (4.6-2.0 V) was also used in Kim and his-co-worker's work [49].

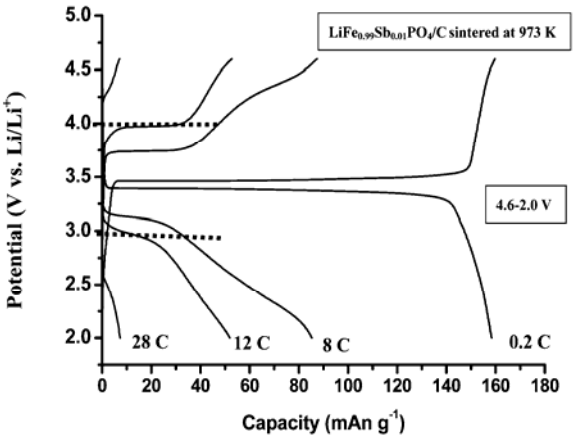

Figure 16: Initial charge and discharge curves for $LiFe_{0.99}Sb_{0.01}PO_4/C$ composites sintered at 973 K under different rates.

4 Conclusions

$LiFePO_4$ was converted to a p-type semiconductor upon Sb-doping, resulting in enhanced electronic conductivity. Among the materials studied, the $LiFe_{0.99}Sb_{0.01}PO_4/C$ composite treated with 36 wt.% sebacic acid demonstrated the best cell performance with a discharge capacity of 154 mAh g^{-1} cycled between 2.8 and 4.0 V at a 0.2 C-rate. Such a significant improvement was mainly attributed to enhanced electronic conductivity from 5.87×10^{-6} to 8.79×10^{-4} S cm^{-1} for the Sb-doped samples. The optimum sintering temperature and duration for preparing the Sb-doped composites were 873 K and 8 hours, respectively. Confirmation of carbon coating and Sb-doping in the composite products was achieved by elemental mapping and EDS analysis. The capacity loss at higher sintering temperatures was caused by the aggregation of composite particles, which decreased surface area and limited the diffusion of lithium ions. However, the in-situ formation of Fe_2P at high temperatures (above 923 K) in $LiFePO_4$ could enhance the discharge capacity at a high C-rate. The $LiFe_{0.99}Sb_{0.01}PO_4/C$ treated at 973 K could sustain a 28 C-rate between 4.6 and 2.0 V, and this rate capability is equivalent to charge or discharge in 129 seconds.

References

[1] S. Tajimi, Y. Ikeda, K. Uematsu, K. Toda, M. Sato, *Enhanced electrochemical performance of $LiFePO_4$ prepared by hydrothermal reaction*, Solid State Ionics 175(2004), 287-290.

[2] A.K. Padhi, K.S. Nanjundaswamy, J.B. Goodenough, *Phospho-olivines as Positive-Electrode Materials for Rechargeable Lithium*

Batteries, J. Electrochem. Soc., 144(1997), 1188-1194.

[3] H. Huang, S.C. Yin, L.F. Nazar, *Approaching Theoretical Capacity of $LiFePO_4$ at Room Temperature at High Rates*, Electrochem. Solid State Lett., 4(2001), A170-A172.

[4] P.P. Prosini, M. Carewska, S. Scaccia, P. Wisniewski, S. Passerini, M. Pasquali, *A New Synthetic Route for Preparing $LiFePO_4$ with Enhanced Electrochemical Performance*, J Electrochem Soc, 149(2002), A886-A890.

[5] J. Barker, M.Y. Saidi, J.L. Swoyer, *Lithium Iron (II) Phospho-olivines Prepared by a Novel Carbothermal Reduction Method*, Electrochem. Solid State Lett., (2003)6, A53-A55.

[6] S. Franger, F.L. Cras, C. Bourbon, H. Rouault, *$LiFePO_4$ Synthesis Routes for Enhanced Electrochemical Performance*, Electrochem. Solid State Lett., (2002)5, 231-233.

[7] S. Okada, S. Sawa, M. Egashira, J.I. Yamaki, M. Tabuchi, H. Kageyama, T. Konishi, A. Yoshino, *Cathode properties of phospho-olivine $LiMnPO_4$ for lithium secondary batteries*, J. Power Sources 97(2001), 430-432.

[8] J. Shim J, K.A. Striebel, *Cycling performance of low-cost lithium ion batteries with natural graphite and $LiFePO_4$*, J. Power Sources, 119(2003), 955-958.

[9] S.T. Myung, S. Komaba, N. Hirosaki, H. Yashiro, N. Kumagai, *Emulsion drying synthesis of olivine $LiFePO_4$/C composite and its electrochemical properties as lithium intercalation material*, Electrochim. Acta 9(2004), 4213-4222.

[10] K. Amine, J. Liu J, I. Belharouak, *High-temperature storage and cycling of C-$LiFePO_4$/graphite Li-ion cells*, Electrochem Commun, 7(2005), 669-673.

[11] D.D. MacNeil, Z. Lu, Z. Chen, J.R. Dahn, *A comparison of the electrode/electrolyte reaction at elevated temperatures for various Li-ion battery cathodes*, J. Power Sources, 108(2002) 8-14.

[12] A.S. Anderesson, J.O. Thomas, *The source of first-cycle capacity loss in $LiFePO_4$*, J. Power Sources, 97(2001) 498-502.

[13] F. Croce F, A.D. Epifanio, J. Hassoun, A. Deptula, T. Olczac, B. Scrosati, *A Novel Concept for the Synthesis of an Improved $LiFePO_4$ Lithium Battery Cathode*, Electrochem. Solid-State Lett., 5(2002), A47-A50.

[14] G. Arnold, J. Garche, R. Hemmer, S. Strobele, C. Volger, M. Wohlfart-Mehrens, *Fine-particle lithium iron phosphate $LiFePO_4$ synthesized by a new low-cost aqueous precipitation technique*, J. Power Sources, 119(2003), 247-251.

[15] K.S. Park, J.T. Son, H.T. Chung, S.J. Kim, C.H. Lee, K.T. Kang, H.G. Kim, *Surface modification by silver coating for improving electrochemical properties of $LiFePO_4$*, Solid State Commun., 129(2004), 311-314.

[16] Z. Chen, J.R. Dahn, *Reducing Carbon in $LiFePO_4$/C Composite Electrodes to Maximize Specific Energy, Volumetric Energy, and Tap Density*, J. Electrochem. Soc., 149(2002), A1184-A1189.

[17] A.S. Andersson, B. Kalska B. L. Häggström, J.O. Thomas, *Lithium extraction / insertion in $LiFePO_4$:an X-ray diffraction and Mossbauer spectroscopy study*, Solid State Ionics, 130(2000), 41-52.

[18] M. Thackeray, *An unexpected conductor*, Nature Mater., 1(2002) 81-82.

[19] P.P. Prosini, M. Lisi, D. Zane, *M. Pasquali, Determination of the chemical diffusion coefficient of lithium in $LiFePO_4$*, Solid State Ionics, 148(2002), 45-51.

[20] H. Huang, S.C. Yin, L.F. Nazar, *Approaching Theoretical Capacity of $LiFePO_4$ at Room Temperature at High Rates*, Electrochem. Solid State Lett., 4(2001), A170-A172.

[21] K.F. Hsu, S.Y. Tsay, B.J. Hwang, *Synthesis and characterization of nano-sized $LiFePO_4$ cathode materials prepared by a citric acid-based sol–gel route, J. Mater. Chem.*, 14(2004), 2690-2695.

[22] R. Dominko, R. Bele, M. Gaberscek, M. Remskar, D. Hanzel, S. Pejovnik, J. Jamnik, *Impact of the Carbon Coating Thickness on the Electrochemical Performance of LiFePO4 OC Composites*, J. Electrochem. Soc., 152(2005) A607-A610.

[23] S.Y. Chung, J.T. Blocking, Y.M. Chiang, *Electronically conductive phospho-olivines as lithium storage electrodes*, Nature Mater., 1(2002), 123-128.

[24] S.Y. Chung, Y.M. Chiang, *Microscale Measurements of the Electrical Conductivity of Doped $LiFePO_4$*, Electrochem. Solid State Lett., 6(2003), A278-A281.

[25] G.X. Wang, S. Bewlay, J. Yao, J.H. Ahn, S.X. Dou, H.K. Liu, *Characterization of $LiM_xFe_{1-x}PO_4$ (M=Mg, Zr, Ti) Cathode Materials Prepared by the Sol-Gel Method*, Electrochem. Solid State Lett., 7(2004), A503-A506.

[26] A. Yamada, S.C. Chung, K. Hinokuna, *Optimized $LiFePO_4$ for Lithium Battery Cathodes*, J. Electrochem. Soc., 148(2001) A224-A229.

[27] S. Franger, F.L. Cras, C. Bourbon, H. Rouault, *$LiFePO_4$ Synthesis Routes for Enhanced Electrochemical Performance*, Electrochem. Solod State Lett., 5(2002) A231-A233.

[28] K.S. Park KS, J.T. Son, H.T. Chung, S.J. Kim, C.H. Lee, H.G. Kim, *Synthesis of $LiFePO_4$ by co-precipitation and microwave heating*, Electrochem. Commun. 5(2003), 839-842.

[29] T.H. Cho, H.T. Chung, *Synthesis of olivine-type $LiFePO_4$ by emulsion-drying method*, J. Power Sources, 133(2004), 272-276.

[30] A. Nytén A, J.O. Thomas, *A neutron powder diffraction study of $LiCo_xFe_{1-x}PO_4$ for x=0, 0.25, 0.40, 0.60 and 0.75*, Solid State Ionics 177(2006), 1327-1330.

[31]C.Y. Ouyang, S.Q. Shi, Z.X. Wang, H. Li, X.J. Huang, L.Q. Chen, *The effect of Cr doping on Li ion diffusion in $LiFePO_4$ from first principles investigations and Monte Carlo simulations*, J. Phys.: Condens. Matter., 16(2004), 2265-2272.

[32]J. Ying, M. Lei, C. Jiang, C. Wan, X. He, J. Li, L. Wang, J. Ren, *Preparation and characterization of high-density spherical $Li_{0.97}Cr_{0.01}FePO_4/C$ cathode material for lithium ion batteries*, J. Power Sources158(2006), 543-549.

[33]D. Wang, H. Li, S. Shi, X. Huang, L. Chen, *Improving the rate performance of $LiFePO_4$ by Fe-site doping*, Electrochim. Acta, 50(2005), 2955-2958.

[34]J. Hong, C. Wang, U. Kasavajjula, *Kinetic behavior of $LiFeMgPO_4$ cathode material for Li-ion batteries*, J. Power Sources, 162(2006), 1289-1296.

[35]D.X. Gouveia, V. Lemos, J.A.C. Paiva, A.G.S. Filho, J.M. Filho, *Spectroscopic studies of Li_xFePO_4 and $Li_xM_{0.03}Fe_{0.97}PO_4$ (M = Cr,Cu,Al,Ti)*, Phys. Rev. B: Condens. Matter., 72(2005) 024105-1~024105-6.

[36]J. Molenda, W. Ojczyk, K. Świerczek, W. Zając, F. Krok, J. Dygas, R.S. Liu, *Diffusional mechanism of deintercalation in $LiFe_{1-y}Mn_yPO_4$ cathode material*, Solid State Ionics, 177(2006), 2617-2624.

[37]C.H. Mia, X.G. Zhang, X.B. Zhaob, H.L. Li, *Synthesis and performance of $LiMn_{0.6}Fe_{0.4}PO_4$/nano-carbon webs composite cathode*, Mater. Sci. Eng. B, 129(2006), 8-13.

[38]T. Nakamura, Y. Miwa, M. Tabuchi, Y. Yamada, *Structural and Surface Modifications of $LiFePO_4$ Olivine Particles and Their Electrochemical Properties*, J. Electrochem. Soc., 153(2006), A1108-A1114.

[39]M. Zhang, L.F. Jiao, H.T. Yuan, Y.M. Wang, J. Guo, M. Zhao, W. Wang, X.D. Zhou, *The preparation and characterization of olivine $LiFePO_4/C$ doped with MoO_3 by a solution method*, Solid State Ionics, 177(2006), 3309-3314.

[40]H. Liu, Q. Liu, L.J. Fu, C. Li, Y.P. Wu, H.Q. Wu, *Doping effects of zinc on $LiFePO_4$ cathode material for lithium ion batteries*, Electrochem. Commun., 8(2006) 1553-1557.

[41]C.M. Julien, K. Zaghib, A. Mauger, M. Mauger, A. Ait-Salah, M. Selmane, F. Gendron, *Characterization of the carbon coating onto $LiFePO_4$ particles used in lithium batteries*, J. Appl. Phys., 100(2006) 063511-1~065311-7.

[42]B.D. Cullity, S.R. Stock, *Elements of X-ray Diffraction 3rd ed*, Prentice Hall Publishers, NJ USA, 2001

[43]W. Ojczyk, J. Marzec, K. Swierczek, W. Zaj, M. Molenda, R. Dziembaj, J. Molenda, *Studies of selected synthesis procedures of the conducting $LiFePO_4$-based composite cathode materials for Li-ion batteries*, J. Power Sources, 173(2007), 700-706.

[44]S.J. Kwon, C.W. Kim, W.T. Jeong, K.S. Lee, *Synthesis and electrochemical properties of olivine $LiFePO_4$ as a cathode material prepared by mechanical alloying*, J. Power Sources 137(2004), 93-99.

[45]G.T.K. Fey, T.L. Lu, *Morphological characterization of $LiFePO_4/C$ composite cathode materials synthesized via a carboxylic acid route*, J. Power Sources, 178(2008), 807-814.

[46]H. Xie, Z. Zhou, *Physical and electrochemical properties of mix-doped lithium iron phosphate as cathode material for lithium ion battery*, Electrochim. Acta, 51(2006), 2063-2067.

[47]G.T.K. Fey, Y.G. Chen, H.M. Kao, *Electrochemical properties of $LiFePO_4$ prepared via ball-milling*, J. Power Sources 189(2009), 169-178.

[48]H.C. Kang, D.K. Jun, B. Jin, E.M. Jin, K.H. Park, H.B. Gu, K.W. Kim, *Optimized solid-state synthesis of $LiFePO_4$ cathode materials using ball-milling*, J. Power Sources 179(2008), 340-346.

[49]J.K. Kim, G. Cheruvally, J.W. Choi, J.U. Kim, J.H. Ahn, G.B. Cho, K.W. Kim, H.J. Ahn, *Effect of mechanical activation process parameters on the properties of $LiFePO_4$ cathode material*, J. Power Sources, 166(2007), 211-218.

Primary Author

George Ting-Kuo Fey, Chair Professor of Chemical and Materials Engineering at National Central University, Taiwan, R.O.C. He received the Ph D. degree in Inorganic Chemistry, University of Massachusetts, 1973. Recent work has been in the fields of high-voltage cathode materials, lithium mixed metal oxides, coating methods for cathode materials, and development of $LiFePO_4$ for high-power lithium-ion cells.